BJP British Journal of Pharmacology

DOI:10.1111/bph.12683
www.brjpharmacol.org

RESEARCH PAPER

A study of the molecular mechanism of binding kinetics and long residence times of human CCR5 receptor small molecule allosteric ligands

David C Swinney[1,2], Paul Beavis[1], Kai-Ting Chuang[1], Yue Zheng[1], Ina Lee[1], Peter Gee[1], Jerome Deval[1], David M Rotstein[1], Marianna Dioszegi[1], Palani Ravendran[1], Jun Zhang[1], Surya Sankuratri[1], Rama Kondru[1] and Georges Vauquelin[3]

[1]*Roche Palo Alto, Palo Alto, CA, USA,* [2]*Institute for Rare and Neglected Diseases Drug Discovery, Mountain View, CA, USA, and* [3]*Department of Molecular and Biochemical Pharmacology, Vrije Universiteit Brussel, Brussels, Belgium*

Correspondence
David Swinney, Institute for Rare and Neglected Diseases Drug Discovery, 897 Independence Ave., Suite 2C, Mountain View, CA 94043, USA. E-mail: david.swinney@irnd3.org

Keywords
CCR5; HIV-1 infection; maraviroc; binding kinetics; pharmacology; molecular mechanism of action; allosteric

Received
6 October 2013
Revised
4 February 2014
Accepted
26 February 2014

BACKGROUND AND PURPOSE
The human CCR5 receptor is a co-receptor for HIV-1 infection and a target for anti-viral therapy. A greater understanding of the binding kinetics of small molecule allosteric ligand interactions with CCR5 will lead to a better understanding of the binding process and may help discover new molecules that avoid resistance.

EXPERIMENTAL APPROACH
Using [^{3}H] maraviroc as a radioligand, a number of different binding protocols were employed in conjunction with simulations to determine rate constants, kinetic mechanism and mutant kinetic fingerprints for wild-type and mutant human CCR5 with maraviroc, aplaviroc and vicriviroc.

KEY RESULTS
Kinetic characterization of maraviroc binding to the wild-type CCR5 was consistent with a two-step kinetic mechanism that involved an initial receptor–ligand complex (RA), which transitioned to a more stable complex, R'A, with at least a 13-fold increase in affinity. The dissociation rate from R'A, k_{-2}, was 1.2×10^{-3} min^{-1}. The maraviroc time-dependent transition was influenced by F85L, W86A, Y108A, I198A and Y251A mutations of CCR5.

CONCLUSIONS AND IMPLICATIONS
The interaction between maraviroc and CCR5 proceeded according to a multi-step kinetic mechanism, whereby initial mass action binding and later reorganizations of the initial maraviroc–receptor complex lead to a complex with longer residence time. Site-directed mutagenesis identified a kinetic fingerprint of residues that affected the binding kinetics, leading to the conclusion that allosteric ligand binding to CCR5 involved the rearrangement of the binding site in a manner specific to each allosteric ligand.

Abbreviations
APL, aplaviroc, GSK 873140; MCV, maraviroc, UK 427,857; NSB, non-specific binding; SPA, scintillation proximity assays; VCV, vicriviroc, SCH-D

Introduction

The human CCR5 receptor) is a co-receptor for HIV-1 entry into CD4+ T-cells (Fatkenheuer *et al.*, 2005; receptor nomenclature follows Alexander *et al.*, 2013). The importance of CCR5 to HIV-1 infection was discovered by the observation that naturally occurring polymorphisms of the *CCR5* gene provide resistance to infection (Liu *et al.*, 1996). HIV-1 entry requires sequential interactions of the viral envelope glycoprotein, gp120, with CD4 and a co-receptor, either CCR5 or CXCR4.

Mutagenesis and modelling studies have provided insights into the molecular mechanism of small molecules binding to CCR5 (Dragic *et al.*, 2000; Tsamis *et al.*, 2003; Fano *et al.*, 2006; Maeda *et al.*, 2006; Kondru *et al.*, 2008). An increased understanding of the molecular mechanism(s) may help with the design of new medicines as HIV-1 develops resistance to the conformations induced by the current drugs. Allosteric ligands of CCR5, including miroviroc (MVC), vicriviroc (VCV) and aplaviroc (APL), bind in a lipophilic pocket with high affinity and very slow dissociation rates. The different allosteric ligands bind to similar but not completely identical sites near the extracellular surface of the receptor between the transmembrane helices (Watson *et al.*, 2005; Seibert *et al.*, 2006).

The molecular mechanism of allosteric modulation was proposed to involve formation of one or more ligand–receptor conformers that are less suitable to interact with gp120 (HIV-1) (Maeda *et al.*, 2006; Garcia-Perez *et al.*, 2011a). All docking poses as well as mutagenesis results are consistent with MVC binding to CCR5 to cause conformational rearrangements of extracellular domains rather than by simple steric hindrance. The consensus mechanism is that MVC binding induced conformational rearrangements that alter interaction between extracellular loop 2 of CCR5 and the V3 loop of gp120. This is further supported by the observation that MVC accelerated dissociation of [^{125}I]-CCL3 and [^{35}S]-gp120 from CCR5 (Garcia-Perez *et al.*, 2011a).

MVC binding to CCR5 has been reported by Napier and co-workers to have a dissociation half-life of greater than 6 h (Napier *et al.*, 2005). This observation of slow-binding kinetics is not surprising in light of the dynamic conformational changes implied in the mechanistic studies described earlier. The slow kinetics has been suggested to explain discrepancies between equilibrium binding assays and function response. Garcia-Perez *et al.* (2011a) noted that TAK779 was threefold less potent than MVC for competing with the binding of [^{35}S]-gp120 to CCR5 but more than 100-fold less potent than MVC at inhibiting HIV-1 entry and replication. They noted that MVC has a prolonged residence time as compared to TAK779, which they suggested may account for this difference.

It is clear that allosteric ligands bind to CCR5 in a dynamic manner involving conformational changes that are associated with slow-binding kinetics. The studies noted earlier described structural features of the binding. However, much less is known about the features that affect the binding kinetics. The characterization of binding kinetics to better understand how potential drugs bind with their target is an emerging area of interest (Swinney, 2004; 2006; 2009; Copeland *et al.*, 2006; Vauquelin *et al.*, 2006; 2012; Copeland, 2010; Lu and Tonge, 2010) and the development of new methods and information that increases this understanding is of interest.

In this report, we present some of our studies and findings on the binding kinetics associated with MVC, VCV and APL binding to recombinant human CCR5 in CHO cell membranes. Comparison of the results obtained by different experimental radioligand binding protocols as well as simulation studies (presented in the Supporting Information) led to the conclusion that MVC, and most likely also APL and VCV, binds to the wild-type (WT) CCR5 receptor according to a multi-step binding mechanism. Site-directed mutagenesis studies were conducted to obtain a kinetic binding fingerprint for each of the antagonists and showed that they were distinct for MVC, APL and VCV.

Methods

Materials and reagents

The CCR5 small-molecule ligands MVC, VCV and APL were synthesized at Roche Palo Alto, Palo Alto, CA, USA. [^{3}H]-MVC was prepared to a specific activity of 70.67 Ci·mmol^{-1} by the Roche Palo Alto radiochemistry group. CCR5 and site-directed mutants were prepared as previously described by Kondru *et al.* (2008). Binding studies were performed at room temperature (i.e. 22–25°C) using membranes from CHO cells that express human WT or mutant CCR5. The concentration of the WT receptors in membranes, determined from saturation experiments, ranged from 8 to 36.3 pmol·mg^{-1} protein. The concentrations of mutant receptors ranged between 1 and 20 pmol·mg^{-1} protein.

Filtration-based [^{3}H]-MVC binding protocols

General. WT or mutant CCR5 bearing CHO cell membranes were incubated in V-bottom 96-well plates (Greiner Bio-One, Monroe, North California, USA) in 200 µL (final volume) of binding buffer with [^{3}H]-MVC either alone or in the presence of the indicated final concentrations of unlabelled antagonists (for 'total' binding) or with the same concentration of [^{3}H]-MVC and 20 µM (final concentration) unlabelled MVC (for 'non-specific' binding). Binding buffer was composed of 20 mM HEPES (pH 7.2), 2 mM $CaCl_2$, 5 mM KCl and 0.02% sodium azide. The amount of membranes used ranged between 6 and 20 µg/200 µL well depending upon receptor expression levels. The assay was terminated using a 96-well Filtermate Harvester (PerkinElmer, Boston, MA, USA) by filtration of the reaction onto a UniFilter-96 GF/B (PerkinElmer) membrane pre-treated with 0.5% polyethyleneimine. The UniFilters were washed five times with ice-cold buffer containing 25 mM HEPES (pH 7.1), 1 mM $CaCl_2$ and 5 mM $MgCl_2$. The UniFilters were then dried over night at room temperature and 40 µL microscint-20 (PerkinElmer) was added to each well. The UniFilter plates were sealed and counted in counts per min (cpm) to quantify the fraction of bound [^{3}H]-MVC remaining on the membrane. 'Specific' CCR5-related binding was calculated by subtracting the non-specific binding (NSB) cpm from the total binding cpm. The specific activity in cpm·pmol^{-1} was determined in each

experiment by counting a known amount of [^{3}H]-MVC, this specific activity was used to convert the binding cpm to pmol.

Saturation binding of [^{3}H]-MVC. Receptors were incubated with increasing concentrations of [^{3}H]-MVC for 3 h at RT. Specific binding was plotted against the [^{3}H]-MVC concentration and the total receptor concentration (i.e. B_{max}, in pmol·mg^{-1} protein) and equilibrium dissociation constant (K_D) were calculated by non-linear regression analysis according to a one-site hyperbolic function in GraphPad Prism 4 (Intuitive Software, San Diego, CA, USA). The receptor concentrations were sufficiently below the K_D values that ligand depletion would not be a factor in the results.

Competition binding ('kinetic shift' protocol). The unlabelled compounds were dissolved in 100% DMSO. For the 'classical' competition binding protocol, receptors were co-incubated for 2 h with a fixed concentration (typically 4 nM, approximately 3 × K_D) of [^{3}H]-MVC either alone (for control binding) or in the presence of increasing concentrations of unlabelled compounds. The 'kinetic shift' protocol included a second experimental 'branch' wherein receptors were pre-incubated for 3 h with increasing concentrations of unlabelled compounds and then co-incubated for 2 h with the unlabelled antagonists along with a fixed concentration (as described earlier) of [^{3}H]-MVC. Concentrations that reduced control binding by 50% (i.e. IC_{50}) were calculated using the sigmoidal dose–response model with one binding site in Microsoft XLfit. Apparent equilibrium dissociation constants (denoted as K_I for the co-incubation branch and as K_I* for the pre-incubation branch) were calculated from the corresponding IC_{50} values according to the Cheng and Prusoff (1973) equation using the K_D of [^{3}H]-MVC obtained from saturation binding for the appropriate receptor species.

Association and direct dissociation of [^{3}H]-MVC. [^{3}H]-MVC association rates were determined by incubation with different concentrations (typically 1–20 nM) for increasing time periods, after which binding is measured. The pseudo-first-order association rate constant (k_{obs}) for each concentration was calculated in GraphPad Prism 4 by non-linear regression analysis of the specific binding versus incubation time plot according to a one-phase exponential association paradigm.

The dissociation profiles of [^{3}H]-MVC were determined by pre-incubating the receptors for 3 h with 3.9 nM of radioligand. The washout phase was initiated by diluting the pre-incubated mixture fivefold and adding 20 μM unlabelled MVC. Specific [^{3}H]-MVC binding was recorded after different time periods, expressed in percentage of control binding (i.e. specific binding at the onset of the washout) and plotted against the washout time. The first-order dissociation rate constant (k_{off}) was calculated by GraphPad Prism 4 from this plot according to a one- or two-phase exponential dissociation paradigm.

Scintillation proximity assays (SPA)

The dissociation rate constants of unlabelled MVC, VCV and APL were determined indirectly by a 'delayed radioligand association' protocol that we developed with the use of a continuous SPA technology using the LeadSeeker imaging system (GE Healthcare, Piscataway, NJ, USA). Wheatgerm agglutinin, polystyrene coupled imaging beads (GE Healthcare) were shaken vigorously with receptor bearing membrane preparations at a concentration ratio of 7.5 μg protein per 0.5 mg bead in the dark for 2 h. Samples (40 μL) of this mixture were then added to a 384-well plate and pre-incubated in the dark for 4 h with 10 μL of buffer only (as control), 10 μL of unlabelled antagonist solution at a concentration equal to three times the previously determined K_I. NSB values were determined for each receptor species by the addition of unlabelled MVC (20 μM final concentration). This pre-incubation phase was followed by the transfer of 40 μL of highly concentrated [^{3}H]-MVC (final concentration 25 times its K_D) using the Multimek 384-well automated pipettor. This operation also produced a fivefold dilution of the unlabelled antagonist. [^{3}H]-MVC binding, as given by the luminescence of the beads, was recorded after different time periods over a 24 h span. As the system did not have fluidics, there was a 1–2 min delay in collecting data after the addition of [^{3}H]-MVC due to the time required to manually transfer the plates from the Multimek to the Leadseeker. The data were normalized to wells with no added competitor to account for changes in the binding during the time of the experiment. In general, this was minimal.

Results

Premise for the calculation of experimental binding parameters

All calculations are based upon the assumption that receptor binding corresponds to a simple reversible bimolecular process that obeys the law of mass action such schematically represented for the 'Single-step bimolecular binding process' in Figure 1. As explicitly outlined in the Supporting Information, the present experimental data are likely to represent multi-step mechanisms (at least two steps) and/or hemi-equilibrium situations. Hence, the rate constants and equilibrium dissociation rate constant that are derived from these experimental data should be considered to be only apparent. To distinguish this model from the more complex 'Two-step bimolecular binding process', the constants that are associated with both models are denominated differently (Figure 1).

Binding kinetics of wild-type CCR5 receptors

The first series of experiments were aimed at investigating the association and dissociation binding profile of [^{3}H]-MVC to membranes from CHO cells that overexpress wild-type human CCR5. Binding of [^{3}H]-MVC to WT CCR5 was saturable in a 3 h experiment (Figure 2A). The experiment shown in Figure 2A is one of the multiple saturation experiments conducted with MCV. The batch of membranes containing CCR5 used in this experiment had a B_{max} of 36.3 pmol·mg^{-1} and the K_D was 1.7 nM.

Association kinetics were determined in experiments where the time-dependent progress of CCR5 binding was monitored at different [^{3}H]-MVC concentrations. As depicted in Figure 2B, binding reached equilibrium between 10 and

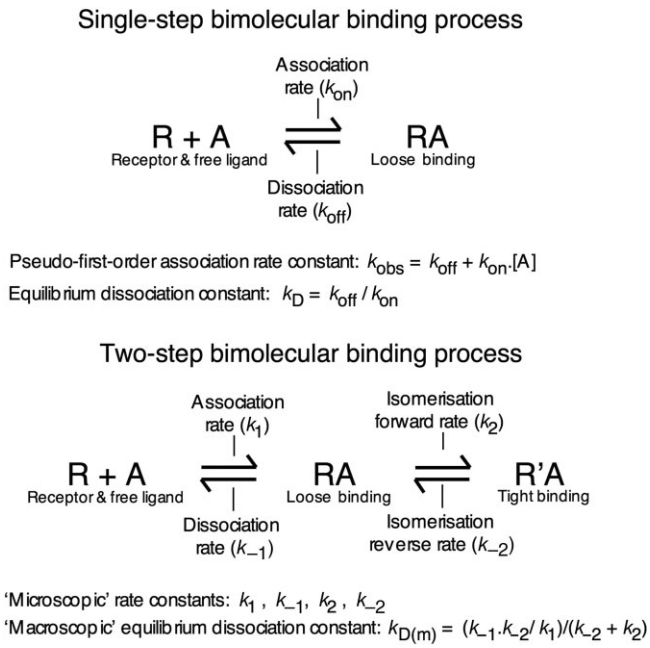

Figure 1

Kinetic mechanisms. Both models are based upon the assumption that receptor binding corresponds to a simple reversible bimolecular process that obeys the law of mass action. Bound receptors can only adopt a single state/conformation in the 'Single-step bimolecular binding process'. In the more complex 'Two-step bimolecular binding process', the initial binding step, yielding a loosely bound complex RA, is followed by a reversible isomerization step yielding a more tightly bound complex R'A. The rate constants that are associated with this latter model are usually defined as 'microscopic' and, to avoid potential confusion, they are denominated differently from those that are associated to the first model.

60 min (at the lowest concentrations). Assuming that this binding corresponds to a reversible bimolecular process that obeys the law of mass action and that bound receptors can only adopt a single state/conformation schematically represented in Figure 1, the pseudo-first-order association rate constant (i.e. k_{obs}, in min^{-1}) should be related to [A] and the association and dissociation rate constants (i.e. k_{on}, in $M^{-1}\cdot min^{-1}$ and k_{off}, in min^{-1}, respectively) as $k_{obs} = k_{off} + k_{on}\cdot[A]$. Compatible with this equation, the k_{obs} versus [A] plot (Figure 2C) is linear. This allows the calculation of k_{on} ($7.8 \pm 0.8 \times 10^6$ $M^{-1}\cdot min^{-1}$) and k_{off} (0.042 ± 0.013 min^{-1}) by linear regression, giving a calculated K_D ($=k_{off}/k_{on}$) of 5.4 nM.

Dissociation kinetics were explored in experiments comprising a 3 h pre-incubation of the receptors with a single concentration of [^{3}H]-MVC, followed by a wash-out in the presence of a 25-fold excess of unlabelled MVC for different time periods up to 24 h (Figure 2D). The time-dependent decline in specific binding during this wash-out fit equally well to both a one-phase model, yielding a k_{off} of 1.8×10^{-3} min^{-1}, and a two-phase model, giving a fast k_{off} of 0.0199 min^{-1} and a slow k_{off} of 1.18×10^{-3} min^{-1} (Figure 2D). The endpoint format of the assay combined with the very long dissociation rate limited the number of time points that were taken during the experiment. The single-step bimolecular binding model requires that both kinetic experiments should yield similar dissociation half-lives. However, the 23-fold difference between the calculated half-lives, 17 min based upon the association experiment and 6.4 h based upon the dissociation experiment, is clearly too large to fit this simple model. Instead, it suggests that the MVC-CCR5 complex may adopt two (or more) states/conformations with distinct stability. This is strongly supported by the continuous 'delayed radioligand association' experiments using an SPA format, in which unlabelled MVC [3.9 nM] was pre-incubated for 2 min, 30 min and 2 h prior to dilution and addition of [^{3}H]-MVC (Figure 2E). The binding of [^{3}H]-MVC requires the unlabelled MVC to dissociate and therefore corresponds to the dissociation phase. Data fitting was clearly more consistent with a two-site model for MVC dissociation with the $k_{-1} = 0.02$ min^{-1} and $k_{-2} = 1.2 \times 10^{-3}$ min^{-1}, corresponding to half-lives of 34 and 552 min respectively. Comparison of the different curves reveals that the fraction of slow-dissociating sites increases with the pre-incubation time.

This prompts us to favour a two-step mechanism, where an initial binding event yields an intermediary RA complex and is followed by a slower isomerization step, yielding the more stable R'A complex (schematically represented in Figure 1), as the simplest explanation for the existence of such distinct states. Additionally, this model also allows the existence of a linear relationship between k_{obs} and [A] such as seen in Figure 2C, provided that the RA state is sufficiently stable to survive the short wash step to separate free from bound [^{3}H]-MVC at the end of the incubation period (Supporting Information).

The 'kinetic shift' experiment shown in Figure 2F further supports the notion that MVC-CCR5 complexes are able to adopt a slow-dissociating state. The control branch of this experiment involved a 2 h co-incubation of the receptors with increasing concentrations of unlabelled MVC and a fixed concentration of [^{3}H]-MVC, while the other branch of the experiment comprises a 3 h pre-incubation of the receptor with increasing concentrations of unlabelled MVC followed by a 2 h incubation with a fixed concentration of [^{3}H]-MVC. The 3 h pre-incubation time was used because the generated competition curve was not significantly different with greater pre-incubation times (data not shown). Compared with the control, this latter competition curve is shifted to the left by approximately 13-fold; that is, the IC_{50} shifts from 1.3 nM without pre-incubation to 0.1 nM with pre-incubation. This shift, further denoted as 'kinetic shift', is compatible with a mechanism wherein pre-formed MVC-CCR5 complexes dissociate so slowly that only a small fraction of the involved receptors are liberated during the 2 h co-incubation phase. This situation resembles the 'insurmountability' that pre-bound slow-dissociating antagonists exhibit in functional 'organ bath'-type experiments (Vauquelin *et al.*, 2002; Kenakin *et al.*, 2006).

The dissociation half-lives for VCV and APL from WT CCR5 were 19.4 ± 0.8 and 21 ± 1.8 h, respectively, as indirectly determined in the delayed association experiments with [^{3}H]-MVC in the SPA format using a one-site model (data not shown). The dissociation of these two antagonists proceeds about three times slower than MVC (half-life of 6.4 h), consistent with a greater kinetic shift than MVC (Table 1).

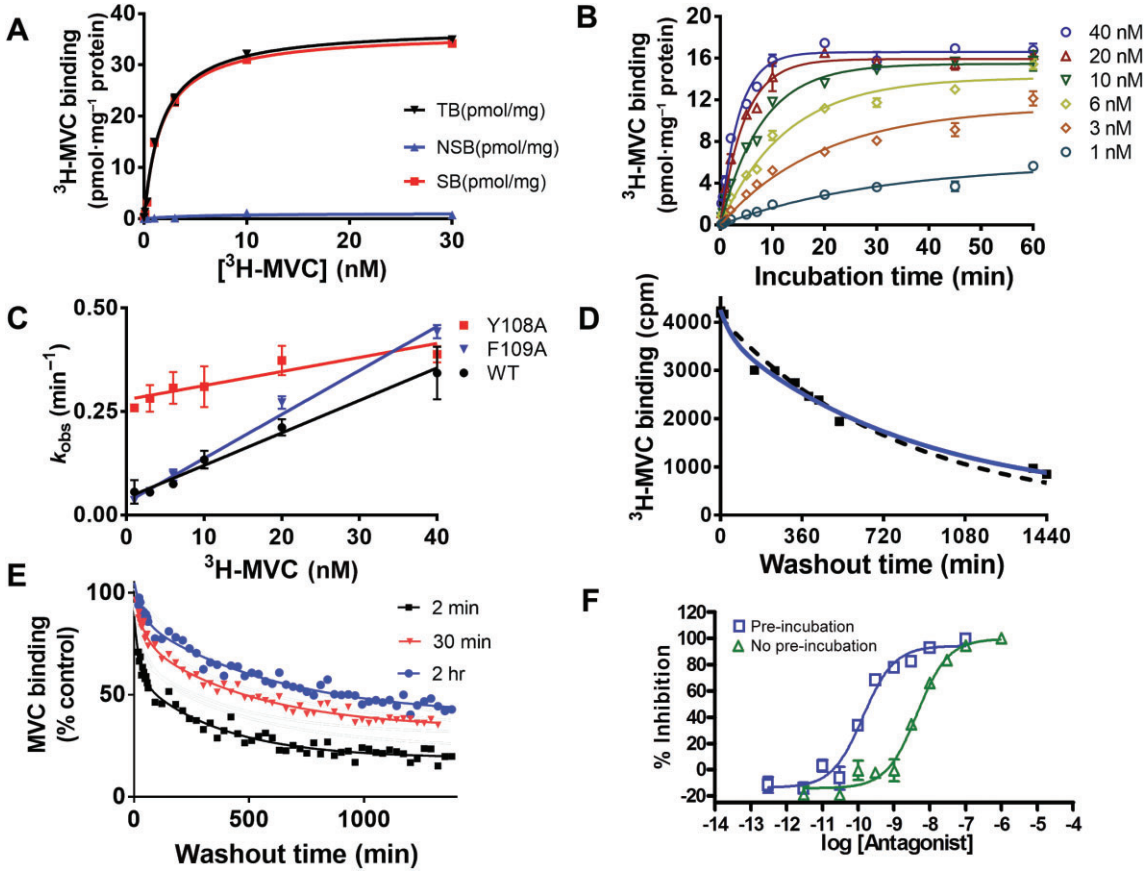

Figure 2

Potency and kinetics of MVC binding to human WT CCR5. (A) Saturation curve of [^{3}H]-MVC binding to human WT CCR5 during 3 h reaction at room temperature. Specific binding was determined by subtracting non-specific binding from total binding. The r^2 for fitting to a one site hyperbolic function for specific binding was 0.993. Binding of [^{3}H]-MVC shown in the ensuing panels is the value for specific binding. (B) Time dependence of association of [1–40 nM] [^{3}H]-MVC with CHO cell membranes containing WT CCR5, the k_{obs} at each concentration was determined by fitting to a single exponential. (C) Kinetic replot of k_{obs} versus [^{3}H]-MVC concentrations for the WT CCR5 and mutants Y108A and F109A. Kinetic constants were determined from the relationship $k_{obs} = k_{on}\cdot[[^3H]\text{-MVC}] + k_{off}$. As shown in the Supporting Information, the relationship between k_{obs} and [[^{3}H]-MVC] is expected to be linear provided that RA state is sufficiently stable to survive the short wash step at the end of the incubation. (D) Pre-incubation of WT CCR5 with [^{3}H]-MVC for 3 h followed by wash-out with 1 μM of unlabelled MVC. Data were fitted to a single and two-phase exponential decay model. (E) Effect of pre-incubation on the dissociation kinetics of MVC. Unlabelled MCV was pre-incubated for 2 min, 30 min and 2 h and dissociation measured continuously after the addition of [^{3}H]-MCV using the SPA format in the Leadseeker. 'Control' refers to the occupancy of CCR5 by MVC at the onset of the washout. (F) 'Kinetic shift' protocol for semi-quantitative estimation of the dissociation rate of unlabelled MVC from WT CCR5. CCR5 were incubated with range of unlabelled MVC concentrations along with 4 nM [^{3}H]-MVC (no pre-incubation) or 3 h prior (pre-incubation) to addition of 4 nM [^{3}H]-MVC. After 2 h at room temperature, the amount of receptor bound [^{3}H]-MVC was determined by filtration.

Binding kinetics of site-specific mutants of CCR5

Site-specific mutations to the allosteric ligand binding site of the human CCR5 were selected based upon previous reports (Dragic *et al.*, 2000; Tsamis *et al.*, 2003; Fano *et al.*, 2006; Maeda *et al.*, 2006; Kondru *et al.*, 2008). The selected residues were located on helices II (F85L, W86A), III (Y108A, F109A), V (T195A, I198A, V199A), VI (W248A, Y251A) and VII (M287A). Mutations on extracellular loops 1 (W94A) and 2 (T177A, S180A) were prepared as well. Membranes from CHO cells that expressed mutated CCR5 were prepared to investigate the effect of the site-specific mutants on the association and saturation binding of [^{3}H]-MVC (Table 1) as well as on the kinetic shift properties of unlabeled MVC, VCV and APL (Table 1). Residues that are essential for high affinity binding are identified as 'hot spots' (underlined data in Table 1) (Wells, 1990). Interestingly, MVC binding required only one hot spot (E283) among the residues that we investigated. No specific [^{3}H]-MVC binding could be detected in our saturation experiments with E283A (data not shown), which is in agreement with published competition binding experiments using [^{125}I]-CCL5 (RANTES), where unlabeled MVC displayed very low potency for this mutant (Table 1) (Kondru *et al.*, 2008). VCV and APL also displayed very low potency in those experiments, indicating that E283 plays a paramount role in the binding of the three CCR5 ligands investigated. All other receptor mutants were able to bind [^{3}H]-MVC with sufficient

Table 1

Potency equilibrium dissociation constants of [^{3}H]-MVC and kinetic shifts by different allosteric ligands for wild-type and mutated CCR5

	[^{3}H] Maraviroc	Maraviroc		Vicriviroc		Aplaviroc	
Receptor species	K_D	K_I	K_I*	K_I	K_I*	K_I	K_I*
WT	1.26 ± 0.37	1.3 ± 0.13	0.097 ± 0.028	7.1 ± 0.90	0.30 ± 0.026	3.7 ± 0.38	0.21 ± 0.05
F85L	1.05 ± 0.26	5.5 ± 0.21	2.9 ± 0.59	40 ± 8.9	29 ± 6.5	67 ± 21	26 ± 7.7
W86A	18.0 ± 0.01	16 ± 11	24	4400 ± 900	5400 ± 6400	1150	980
W94A	0.41 ± 0.04	0.60 ± 0.10	0.043 ± 0.005	3.5 ± 0.42	0.22 ± 0.014	100 ± 22	41 ± 18
Y108A	40.4 ± 2.77	13 ± 3.4	18 ± 9.0	94 ± 16	53 ± 6.3	200 ± 57	45 ± 4.6
F109A	0.92 ± 0.18	0.66 ± 0.081	0.11 ± 0.023	40 ± 6.3	19 ± 9.8	>10 000	>10 000
T177A	0.91	3.7 ± 1.2	0.08 ± 0.03	ND	ND	ND	ND
S180A	0.79	3.0 ± 1.1	0.07 ± 0.01	ND	ND	ND	ND
T195A	1.36 ± 0.47	2.1 ± 0.05	0.24 ± 0.018	11 ± 2.4	0.73 ± 0.087	4.5 ± 1.1	0.40 ± 0.17
I198A	9.19	17 ± 1.5	8.2 ± 1.1	14.5 ± 1.5	6.1 ± 1.6	109	47
V199A	0.58 ± 0.33	4 ± 1.5	0.017 ± 0.006	23 ± 18	0.12 ± 0.058	19 ± 7.2	0.056 ± 0.026
W248A	0.45 ± 0.07	0.51 ± 0.13	0.05 ± 0.009	5.1 ± 1.2	0.17 ± 0.007	3.1 ± 0.54	0.13 ± 0.019
Y251A	4.78	3.9 ± 0.69	1.5 ± 0.57	2.9 ± 0.18	0.38 ± 0.04	1.1	0.076
E283A	No specific binding	18 000[a]	–	98 000[a]	–	603[a]	–
M287A	0.61 ± 0.21	0.56 ± 0.056	0.037 ± 0.004	60 ± 11	26 ± 11	4.5 ± 1.0	0.21 ± 0.069

[^{3}H]-MVC saturation binding experiments were carried out as in Figure 2A to obtain its K_D for the different receptor species after 3 h at room temperature. Apparent equilibrium dissociation constant, K_I: receptors were incubated for 2 h with a range of unlabeled ligand concentrations along with 4 nM [^{3}H]-MVC and curves were analysed according to a sigmoidal dose–response model to yield IC_{50}. K_I values were calculated from the IC50 values and the K_D of [^{3}H]-MVC for the appropriate receptor species according to the Cheng–Prusoff equation. Apparent equilibrium dissociation constant, K_I*: receptors were incubated with range of unlabelled ligand concentrations for 3 h prior to addition of 4 nM [^{3}H]-MVC and further incubation for 2 h. Curves were analysed as outlined earlier. Results are ±SEM. [a]Data obtained from Kondru *et al.* (2008). ND, not done.

affinity to enable their investigation using this radioligand. K_D values of [^{3}H]-MVC, as obtained by saturation binding experiments (3 h incubation), are listed for each mutant in Table 1. Co-incubation competition binding studies revealed an additional hot spot for VCV (W86) and two additional hot spots for APL (W86 and F109) (Table 1).

The effect of the site-specific mutants on dissociation behaviour of unlabelled MVC was determined in competition binding experiments with [^{3}H]-MVC using the kinetic shift protocol described earlier (Table 1). An example of the activity profiles are shown in Figure 3 (right panel) for MVC binding to Y108A where the mutation causes a loss of kinetic shift. The IC_{50} values of unlabelled MVC, VCV and APL that were provided by the co- and pre-incubation branches of these experiments were transformed into apparent K_I values (denoted as K_I and K_I*, respectively) according to the Cheng/Prusoff equation (Cheng and Prusoff, 1973) based upon K_D value of [^{3}H]-MVC for the appropriate mutant receptor determined in the saturation binding experiments (Table 1).

Compared with the WT receptors, the 'kinetic shift' between the competition curves for MVC declined substantially for five site-specific mutants: that is, F85L, W86A, Y108A, I198A and Y251A [Figure 3 (left panel), Figure 4 and Table 1]. It is also only for those five mutants that the curves associated with the pre-incubation protocol yielded appreciably higher K_I* values (i.e. >1.5 nM vs. 0.1 nM) (Table 1). This is likely to be related to the inability of the resulting complexes to adopt a long-lasting high affinity state. Moreover, equilibrium binding of [^{3}H]-MVC was also attained earlier for W86A, Y108A (shown as example in Figure 3, left panel), I198A and Y251A than for the WT receptor (Figure 2B). In Figure 2C, this phenomenon is clearly illustrated by the higher k_{obs} values at low [A] for Y108A and this graphic representation also reveals that this difference is essentially due to the high value of k_{off} (k_{off} = 0.28 ± 0.22 min^{-1}) or, in other words, to the very fast dissociation of the [^{3}H]-MVC-Y108A receptor complex (dissociation $t_{1/2}$ = 2.8 min) (Table 2). This is also observed with W86A (Table 2). Taken together, the different studies with the W86A, Y108A, I198A and Y251A mutants concur with a model wherein these amino acids play an important role in the WT receptor with respect to the formation/stability of the tight binding R'A complex. F85L was the only mutant with a loss of 'kinetic shift' whose association binding profile was similar to that of the WT receptors: that is, k_{on} = 7.0 ± 4.0 × 10^6 M^{-1}·min^{-1} and k_{off} = 0.094 ± 0.093 min^{-1} (Table 2). F85L is proposed to contribute primarily to the transition to R'A but not the formation of RA. Compared with the WT receptors, the 'kinetic shift' was markedly increased with one site-specific mutant (V199A) (Table 1). The 'kinetic shift' and the [^{3}H]-MCV association characteristics were similar to the WT receptor mutants, such as F109A, T195A and W94A (Table 2).

The K_D values determined in the saturation binding experiments (Table 1) and association experiments (Table 2)

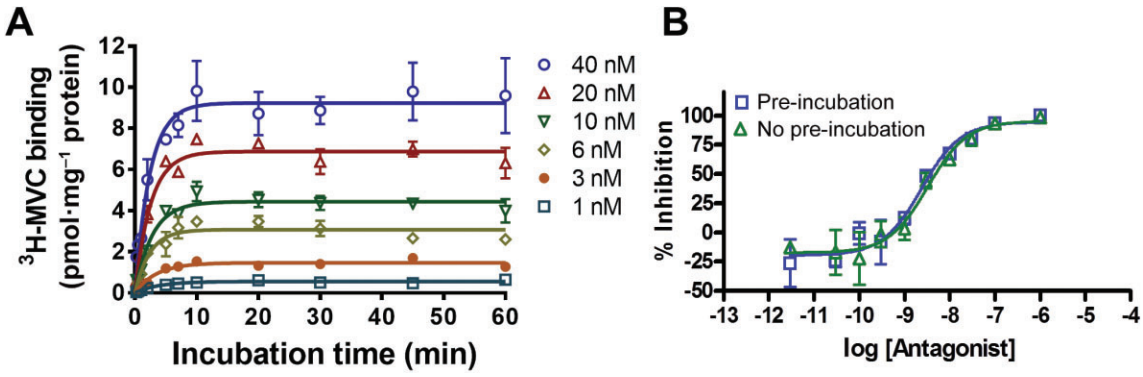

Figure 3

Kinetics of MVC interaction with CCR5 Y108A. Binding of [^{3}H]-MVC in is specific. (A) Time dependence of association of [1–40 nM] [^{3}H]-MVC with CHO cell membranes containing human CCR5Y108A. The k_{obs} at each concentration was determined by fitting to a single exponential. (B) 'Kinetic shift' protocol for semi-quantitative estimation of the dissociation rate of unlabelled MVC from human CCR5-Y108A. The experimental procedure and symbols are the same as outlined in the legend of Figure 2F.

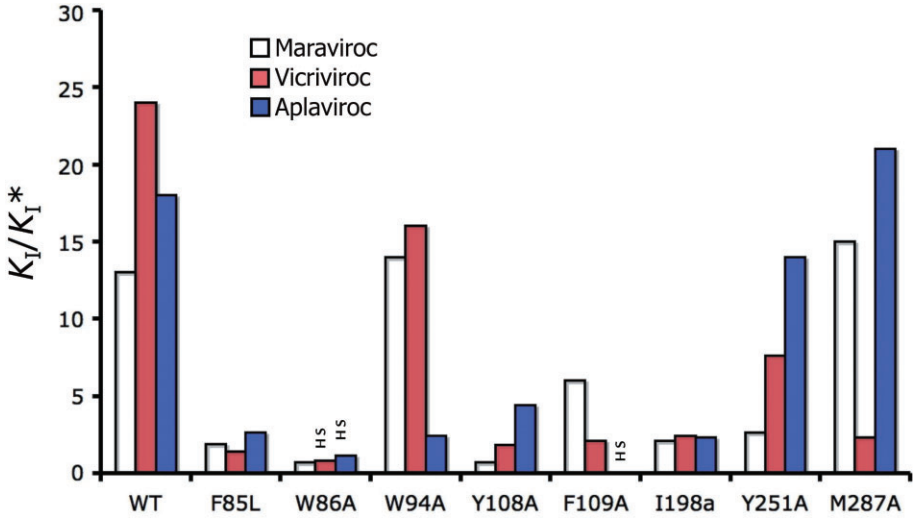

Figure 4

Visual representation of kinetic shifts by different antagonists for WT and mutated CCR5. The ratio of K_I/K_I* quantitates the shift observed upon 3 h pre-incubation and provides a semi-quantitative evaluation of the unlabelled allosteric ligand's residence time. K_I and K_I* values are listed in Table 1. HS, hot spot.

varied by as much as 10-fold. Although some of this variation can be attributed to the larger standard variations for the data determined in the association experiment, it can also be attributed to the challenge of using equilibrium measures in a system that is not at equilibrium (Supporting Information).

Initially, we envisioned measuring the binding kinetics for the individual mutants with MVC, VCV and APL. Table 3 shows the results with MVC and VCV for WT CCR5 and selected mutants determined with the SPA format. Unfortunately, the low affinity of [^{3}H]-MVC for many of the mutants prevented the determination of the k_{-2} due to the high concentrations of [^{3}H]-MVC required for the competition. In addition, we found the kinetic IC_{50} shift assay sufficient to identify the role of specific amino acid residues with satisfactory robustness and throughput. We observed that the dissociation rates for the mutants tested to be consistent with the IC_{50} shift assay. For example, with MVC, the dissociation half-lives for T195A, W94A and W248A were similar to WT as was the IC_{50} shift value, whereas F109A had a much faster dissociation half-life and a corresponding loss of IC_{50} shift. The dissociation rate for APL was similar with T195A and W248A, but decreased with W94A with was also consistent with the loss of IC_{50} shift.

Among the site-specific mutants with a much reduced 'kinetic shift' for MVC, four of them (i.e. F85L, W86A, Y108A and I198A) exhibited the same characteristic for VCV and APL (Figure 4). The reduced 'kinetic shift' for Y251A was more specific for MVC. In the same way, some other non-hot spot reduced 'kinetic shift' mutants also displayed selectivity for VCV (i.e. F109A and M287A) or APL (i.e. W94A). Here again,

Table 2

Kinetic constants for wild-type and mutant CCR5 associated with the time-dependent progress of [^{3}H]-MVC initial binding

Receptor	k_{on} ($M^{-1}\cdot min^{-1}$)	k_{off} (min^{-1})	K_D (nM)
Wild type	$7.8 \pm 0.8 \times 10^6$	0.042 ± 0.013	5.4
Y108A	$3.4 \pm 0.13 \times 10^6$	0.28 ± 0.22	82
W86A	$13 \pm 9.8 \times 10^6$	0.47 ± 0.12	36
F85L	$7.0 \pm 4.0 \times 10^6$	0.094 ± 0.093	13
F109A	$10 \pm 0.9 \times 10^6$	0.021 ± 0.040	2.1
T195A	$4.1 \pm 0.35 \times 10^6$	0.095 ± 0.008	23
W94A	$10 \pm 1.0 \times 10^6$	0.016 ± 0.012	1.6

The time-dependent progress of initial CCR5 binding was monitored at different [^{3}H]-MVC concentrations as described in the Methods section. The k_{on} and k_{off} values are for the initial (or first-step) RA complex formation and dissociation respectively. Results are ±SEM.

Table 3

Dissociation half-lives for selective mutants

CCR5 mutant	MVC, $t_{1/2}$ (min)	APL, $t_{1/2}$ (min)
WT	673.2 ± 53.2	1163.4 ± 45.7
W94A	720.4 ± 83.6	38.4 ± 5.6
F109A	181.8 ± 24.7	ND
T195A	635.0 ± 41.8	1592 ± 709.0
W248A	967.4 ± 207.5	1131.2 ± 25.3

Dissociation half-lives were determined using the SPA protocol described in the Methods section. Membranes were pre-incubated in the dark for 4 h with ligand at a concentration of three times the K_I previously determined. Dissociation from the receptor was initiated by dilution of the ligand by the transfer of 40 µL of [^{3}H]-MVC (final concentration 25 times K_D). The plate was then read over a 24 h period. The rate of dissociation was calculated in terms of the percentage inhibition of [^{3}H]-MVC binding over time when compared to the final specific binding of a buffer only control. k_{off} values for many of the mutants could not be determined for practical reasons as the K_D for MVC binding to the mutants receptors is high such as 40.4 nM for Y108A, then 1.0 µM of [^{3}H]-MVC would be needed for a 25*K_D concentration. Results are ±SEM. ND, not determined.

all these mutants displayed appreciably higher K_I* values for VCV and APL (Table 1). The involved amino acids are therefore also likely to stabilize the tight binding of VCV and APL.

Discussion

This work was initiated to determine if CCR5 allosteric ligands could be differentiated based upon their kinetic binding profiles. It was apparent from the work of Watson *et al.* (2005) that CCR5 allosteric ligands bound in different ways, leading to different functional responses, and a reasonable assumption was that different ligand–receptor conformations interacted differently with gp120 of HIV-1. It was also known that many of the CCR5 ligands had slow dissociation rates. We postulated that ligand-specific conformations would be associated with the slow binding kinetics and that ligands could be differentiated by profiling the amino acids residues involved in the slow binding kinetics. In the course of this work, we undertook detailed kinetic evaluation of MVC, VCV and APL binding to the CCR5 receptor and the results suggest that the allosteric ligands bound in a similar binding site in a ligand-specific manner. We wish to focus the discussion upon two separate aspects of these studies that provided further insights into binding kinetics, the kinetic binding mechanism and the molecular mechanism of slow binding, and to discuss these with respect to the mechanism of inhibition of HIV-1 infection and overcoming resistance.

Kinetic binding mechanism

We concluded the kinetic binding mechanism was a multi-step process. This was supported by the observation that the dissociation half-life of [^{3}H]-MVC and apparent affinity depended upon the pre-incubation time. The dissociation half-life determined in the time-dependent radioligand association experiments with no pre-incubation was 17 min (Figure 2B), whereas the dissociation half-life was much slower (6.4 h) following an initial 3 h pre-incubation of the receptors with the radioligand (Figure 2D and E). This was consistent with the report by Napier *et al.* (2005) that MVC dissociates with a half-life of greater than 6 h. The 23-fold difference between the dissociation half-lives obtained from the association and dissociation experiments cannot be explained by the simplest bimolecular mass action-based binding model in which the ligand–receptor complex adopts a single state or conformation. Instead, it implies that the MVC-CCR5 complex can adopt two (or more) states or conformations with distinct stability. Consistent with this mechanism, we observed the dissociation data from the competitive SPA experimental format to fit a two-phase exponential in which $k_{-1} = 0.02\ min^{-1}$ and $k_{-2} = 1.2 \times 10^{-3}\ min^{-1}$, corresponding to half-lives of 34 min (which is in the same range as the 17 min obtained based on the association kinetic experiment depicted in Figure 2B and C) and 552 min respectively (Figure 2D). It is well accepted that initial bimolecular interactions may be followed by conformational transitions important to a physiological or pharmacological response (Fierens *et al.*, 1999; Vauquelin *et al.*, 2001a,b; Urban *et al.*, 2007; Copeland, 2011). It is likely that the final, stable complex was attained following a succession of conformational transitions.

The shift in apparent affinity with pre-incubation using the 'kinetic shift' experimental protocol was also consistent with a multi-step kinetic mechanism. The methodology for comparing the effect of pre-incubation on the affinity constants of an unlabelled ligand in competition binding experiments was previously used to investigate structural features affecting the dissociation rates of angiotensin AT_1 receptor antagonists (Takezako *et al.*, 2004). With a dissociation half-life for WT CCR5 of greater than 6 h for MVC, and even greater than 18 h for VCV and APL (this study, Napier *et al.*, 2005, Demarest *et al.*, 2008), equilibrium binding can hardly

be reached under the conditions used in this study (Figure 2F). Yet, in spite of this restriction, K_I/K_I* ratios that are derived from such 'kinetic shift' protocol provide a semi-quantitative estimate of an unlabelled drug's time dependence. The ratio is primarily a measure of the relative ratio of forward and reverse isomerization rates (k_2/k_{-2}) (Supporting Information), and consistent with a mechanism involving initial formation of an ligand–receptor complex with affinity around 10 nM, that slowly rearranges to a complex with much slower dissociation rates. In agreement with its slow dissociation in other experiments, MVC displayed a K_I/K_I* ratio of 13 for the WT CCR5 receptor under the present experimental conditions (Table 1). In line with their slower dissociation, even higher ratios were recorded for VCV-24 and APL-17.

An important challenge for this analysis was to clearly differentiate between single and multiple binding states with a binding protocol. Using association experiments alone, it is difficult to distinguish between single state binding and multiple binding states because the experimental protocol only differentiates bound from unbound. However, a change in dissociation rate with incubation time can be diagnostic (Supporting Information). This is in contrast to enzyme assays in which the inhibition is measured by the change in the rate of product formation. In those assays, the slow transition from an initial steady-state velocity to a slower steady-state velocity will be described by curve rate (k_{obs}) versus inhibitor plots for multi-step reactions (Strickland *et al.*, 1975). This feature is known as slow-binding kinetics and has been discussed in detail by Morrison and Walsh (1988).

Molecular mechanism of slow binding

The kinetic results described in this work together with the recently published structure of MVC bound to CCR5 (Tan *et al.*, 2013) and computational studies (Garcia-Perez *et al.*, 2011b) provide a better picture of the molecular mechanism of allosteric ligand slow binding to CCR5. The structure of MVC bound to CCR5 showed the ligand to occupy the bottom of a pocket defined by residues from helices I, II, III, V, VI and VII (Tan *et al.*, 2013). The nitrogen tropane group of MVC was engaged in a salt bridge with E283 and the carboxamide nitrogen forms a hydrogen bond with Y251. The phenyl group reaches deep into the pocket to form hydrophobic interactions with five aromatic residues: Y108, F109, F112, Y248 and Y251. The triazole, tropane and cyclohexane groups also fit into small subpockets and make hydrophobic contacts with CCR5. Many of these residues are involved in the kinetic transition and were previously identified as crucial for HIV-1 infection. Maeda and co-workers reported that Y108, E283 and Y251 were crucial for HIV-1-gp120/sCD4 complex binding and HIV-1 fusion, and proposed that the hydrogen bond network among these transmembrane residues was disrupted with the allosteric inhibitors, presumably leading to the conformational changes that disrupt HIV-1 binding to CCR5 (Maeda *et al.*, 2006). Garcia-Perez *et al.* (2011b) reported that E283 is the only residue essential for MVC binding. They determined that five other residues are important for the definition of the MVC binding site (W86, Y108, Y251, I198 and N194) but the effects of their mutation are most probably not due to the loss of key intermolecular interactions but rather to indirect structural effects. From their computational studies, they concluded there cannot be tight complementarity between the shape of drug and the receptor 7TM cavity in part due to the size of the cavity (Garcia-Perez *et al.*, 2011b). The modelled cavity of the free receptor was found to be wide and deep, and its volume about twice as large as that of MVC. Interestingly, this contrasts with what was observed in the structure reported by Tan *et al.* (2013), where they observed good complementarity between the shape of the drug and receptor.

We observed that many of the same residues contributed to the slow kinetics of MVC binding. A mechanism for the slow binding kinetics consistent with these findings is the rearrangement of the large, flexible binding site to form complementary interactions with the CCR5 ligands. The requirement of E283 for MVC, F109 for APL, and E283 and W86 for VCV suggests that both RA and R'A complexes are in the pocket described in the MVC bound structure of Tan *et al.* (2013). The structural differences between RA and R'A are due to dynamic rearrangement in the same binding pocket. Initial ligand association with the receptor (RA) involves contribution of these anchoring interactions deep in the large CCR5 binding pocket. The RA complex then slowly transitions to a most stable state (R'A). We speculate that the initial dynamic, flexible RA state will sample the conformational space and transition to a more stable, longer lasting state when a transition state complementary to the structure of the small-molecule ligand is identified. The transition state and subsequent final state are unique to each ligand. The ligand-specific interactions are then translated to ligand-specific surface conformations of the receptor that are differentially recognized by the GP120 of HIV-1. We conclude that the differential binding of the antagonists to the CCR5 receptor is determined by contributions from residues that stabilize the binding as well as residues in the transition states to ligand-specific stable complexes (R'A). The design of differentiated molecules requires consideration of both binding determinants. This interpretation of the binding kinetic results concurs with the increasing awareness that GPCRs are flexible and can adopt conformations around ligands. In this respect, Teague (2003) proposed that conformational diversity is influenced by the flexibility of protein structures which allow different pharmacophores to bind in the same region: one binding site, multiple binding arrangements. The so-obtained ligand-specific receptor conformations can have different functions, a behaviour that is known as 'functional selectivity' for agonists (Urban *et al.*, 2007). The pioneering work by Kobilka and co-workers (Ghanouni *et al.*, 2001; Swaminath *et al.*, 2004; Yao *et al.*, 2006; Kobilka and Deupi, 2007; Rasmussen *et al.*, 2007; Rosenbaum *et al.*, 2007; Kobilka and Schertler, 2008) is very revealing in this respect. They demonstrated that the interaction between agonists and GPCRs proceed by kinetically distinguishable steps through discrete intermediate conformational states, implying that each state increases the probability of the subsequent one to be formed. They studied the structure of the β_2-adrenoceptor bound to a slow-dissociating inverse agonist and concluded that each ligand–receptor complex will have unique conformations (Rosenbaum *et al.*, 2007). Similarly, Del Carmine *et al.* (2004) also suggested that the β_2-adrenoceptor agonist binding pocket was not pre-formed, but dynamically assembled as the ligand binds. The dynamics may be an intrinsic property of

the initial encounter complex where the molecules move relative to one another, thereby sampling different conformations rather than being 'induced' (Keeble and Kleanthous, 2005).

Ultimately, HIV-1 will develop resistance and there will be a need for new molecules with different resistance profiles. Molecules that induce unique conformations of the receptor should, in theory, have different resistance profiles. Identification of interactions between the receptor and small molecule that contribute to the unique dynamic transitions could inform chemical design towards changing the binding dynamics while retaining binding affinity. In this case, the slow binding kinetics provide a diagnostic for ligand-specific conformational changes, and the kinetic mutant fingerprint can be used to infer identification of specific interactions associated with ligand-specific conformational changes.

Conflict of interest

None.

Author contributions

David C. Swinney designed the studies and wrote the paper; Paul Beavis, Kai-Ting Chuang, Yue Zheng, Ina Lee and Peter Gee conducted kinetic experiments; Jerome Deval helped with the design and interpret the kinetic experiments; Marianna Dioszegi and Jun Zhang prepared mutant receptors; Palani Ravendran helped with kinetic analysis; David M. Rotstein, Surya Sankuratri and Rama Kondrun contributed to the design and interpretations of studies; and Georges Vauquelin help interpret kinetic analysis and write the paper.

References

Alexander SPH, Benson HE, Faccenda E, Pawson AJ, Sharman JL Spedding M *et al.* (2013). The Concise Guide to PHARMACOLOGY 2013/14: G Protein-Coupled Receptors. Br J Pharmacol 170: 1459–1581.

Cheng Y, Prusoff WH (1973). Relationship between the inhibition constant (K_I) and the concentration of inhibitor which causes 50 per cent inhibition (IC_{50}) of an enzymatic reaction. Biochem Pharmacol 22: 3099–3108.

Copeland R (2010). The dynamics of drug-target interactions: drug-target residence time and its impact on efficacy and safety. Expert Opin Drug Discov 5: 305–310.

Copeland RA (2011). Conformational adaptation in drug-target interactions and residence time. Future Med Chem 3: 1491–1501.

Copeland RA, Pompliano DL, Meek TD (2006). Drug-target residence time and its implications for lead optimization. Nat Rev Drug Discov 5: 730–739.

Del Carmine R, Molanari P, Sbraccia M, Ambrosio C, Costa T (2004). 'Induced-fit' mechanism for catecholamine binding to the beta2-adrenergic receptor. Mol Pharmacol 66: 356–363.

Demarest JF, Sparks SS, Schell K, Shibayama S, McDanal CB, Fang L *et al.* (2008). *In vitro* and clinical investigation of the relationship between CCR5 receptor occupancy and anti-HIV activity of aplaviroc. J Clin Pharmacol 48: 1179–1188.

Dragic T, Trkola A, Thompson DA, Cormier EG, Kajumo FA, Maxwell E *et al.* (2000). A binding pocket for a small molecule inhibitor of HIV-1 entry within the transmembrane helices of CCR5. Proc Natl Acad Sci USA 97: 5639–5644.

Fano A, Ritchie W, Carrieri A (2006). Modeling of the structural basis of human CCR5 chemokine receptor function: from homology model building and molecular dynamics validation to agonist and antagonist docking. J Chem Inf Model 46: 1223–1235.

Fatkenheuer G, Pozniak AL, Johnson MA, Plettenberg A, Staszewski S, Hoeplman AI *et al.* (2005). Efficacy of short-term monotherapy with maraviroc, a new CCR5 antagonist, in patients infected with HIV-1. Nat Med 11: 1170–1172.

Fierens FLP, Vanderheyden PML, De Backer J-P, Vauquelin G (1999). Insurmountable angiotensin II AT1 receptor antagonists: the role of tight antagonist binding. Eur J Pharmacol 372: 199–206.

Garcia-Perez J, Rueda P, Staropoli I, Kellenberger E, Alcami J, Arenzana-Seisdedos F *et al.* (2011a). New insights into the mechanisms whereby low molecular weight CCR5 ligands inhibit HIV-1 infection. J Biol Chem 286: 4978–4990.

Garcia-Perez J, Rueda P, Alcami J, Rognan D, Arenzana-Seisdedos F, Lagane B *et al.* (2011b). Allosteric model of maraviroc binding to CC chemokine receptor 5 (CCR5). J Biol Chem 286: 33409–33421.

Ghanouni P, Gryczynski Z, Steenhuis JJ, Lee TW, Farrens DL, Lakowicz JR *et al.* (2001). Functionally different agonists induce distinct conformations in the G protein coupling domain of the beta 2 adrenergic receptor. J Biol Chem 276: 24433–24436.

Keeble AH, Kleanthous C (2005). The kinetic basis for dual recognition in colicin endonuclease-immunity protein complexes. J Mol Biol 352: 656–671.

Kenakin T, Jenkinson S, Watson C (2006). Determining the potency and molecular mechanism of action of insurmountable antagonists. J Pharmacol Exp Ther 319: 710–723.

Kobilka B, Schertler GF (2008). New G-protein-coupled receptor crystal structures: insights and limitations. Trends Pharmacol Sci 29: 79–83.

Kobilka BK, Deupi X (2007). Conformational complexity of G-protein-coupled receptors. Trends Pharmacol Sci 28: 397–406.

Kondru R, Zhang J, Ji C, Mirzadegan T, Rotstein D, Sankuratri S *et al.* (2008). Molecular interactions of CCR5 with major classes of small-molecule CCR5 antagonists. Mol Pharmacol 73: 789–800.

Liu R, Paxton WA, Choe S, Ceradini D, Martin SR, Horuk R *et al.* (1996). Homozygous defect in HIV-1 coreceptor accounts for resistance of some multiply-exposed individuals to HIV-1 infection. Cell 86: 367–377.

Lu H, Tonge PJ (2010). Drug-target residence time: critical information for lead optimization. Curr Opin Chem Biol 14: 467–474.

Maeda K, Das D, Ogata-Aoki H, Nakata H, Miyakawa T, Tojo Y *et al.* (2006). Structural and molecular interactions of CCR5 inhibitors with CCR5. J Biol Chem 281: 12688–12698.

Morrison JF, Walsh CT (1988). The behavior and significance of slow-binding enzyme inhibitors. Adv Enzymol Relat Areas Mol Biol 61: 201–301.

Napier C, Sale H, Mosley M, Rickett G, Dorr P, Mansfield R *et al.* (2005). Molecular cloning and radioligand binding characterization of the chemokine receptor CCR5 from rhesus macaque and human. Biochem Pharmacol 71: 163–172.

Rasmussen SG, Choi HJ, Rosenbaum DM, Kobilka TS, Thian FS, Edwards PC *et al*. (2007). Crystal structure of the human beta2 adrenergic G-protein-coupled receptor. Nature 450: 383–388.

Rosenbaum DM, Cherezov V, Hanson MA, Rasmussen SG, Thian FS, Kobilka TS *et al*. (2007). GPCR engineering yields high-resolution structural insights into beta2-adrenergic receptor function. Science 318: 1266–1273.

Seibert C, Ying W, Gavrilov S, Tsamis F, Kuhmann SE, Palani A *et al*. (2006). Interaction of small molecule inhibitors of HIV-1 entry with CCR5. Virology 349: 41–54.

Strickland S, Palmer G, Massey V (1975). Determination of dissociation constants and specific rate constants of enzyme-substrate (or protein-ligand) interactions from rapid reaction kinetic data. J Biol Chem 250: 4048–4052.

Swaminath G, Deupi X, Lee TW, Zhu W, Thian FS, Kolilka TS *et al*. (2004). Probing the beta2 adrenoceptor binding site with catechol reveals differences in binding and activation by agonists and partial agonists. J Biol Chem 280: 22165–22171.

Swinney DC (2004). Biochemical mechanisms of drug action: what does it take for success? Nat Rev Drug Discov 3: 801–808.

Swinney DC (2006). Can binding kinetics translate to a clinically differentiated drug? From theory to practice. Lett Drug Des Disc 3: 569–574.

Swinney DC (2009). The role of binding kinetics in therapeutically useful drug action. Curr Opin Drug Discov Devel 12: 31–39.

Takezako T, Gogonea C, Saad Y, Noda K, Karnik SS (2004). Network leaning as a mechanism of insurmountable antagonism of the angiotensin II type 1 receptor by non-peptide antagonists. J Biol Chem 279: 15248–15257.

Tan Q, Zhu Y, Li J, Chen Z, Han GW, Kufareva I *et al*. (2013). Structure of the CCR5 chemokine receptor-HIV entry inhibitor maraviroc complex. Science 341: 1387–1390.

Teague SJ (2003). Implications of protein flexibility for drug discovery. Nat Rev Drug Discov 2: 527–541.

Tsamis F, Gavrilov S, Kajumo F, Seibert C, Kuhmann S, Ketas T *et al*. (2003). Analysis of the mechanism by which the small-molecule CCR5 antagonists SCH-351125 and SCH-350581 inhibit human immunodeficiency virus type 1 entry. J Virol 77: 5201–5208.

Urban JD, Clarke WP, von Zastrow M, Nichols DE, Kobilka B, Weinstein H *et al*. (2007). Functional selectivity and classical concepts of quantitative pharmacology. J Pharmacol Exp Ther 320: 1–13.

Vauquelin G, Fierens F, Verheyen I, Vanderheyden P (2001a). Insurmountable AT1 receptor antagonism: the need for different antagonist binding states of the receptor. Trends Pharmacol Sci 22: 343–344.

Vauquelin G, Morsing P, Fierens FLP, De Backer JP, Vanderheyden PML (2001b). A two-state receptor model for the interaction between angiotensin II AT1 receptors and their non-peptide antagonists. Biochem Pharmacol 61: 277–284.

Vauquelin G, Van Liefde I, Vanderheyden P (2002). Models and methods for studying insurmountable antagonism. Trends Pharmacol Sci 23: 514–518.

Vauquelin G, Fierens F, Van Liefde I (2006). Long-lasting AT_1 receptor binding and protection by candesartan: comparison to other biphenyl-tetrazole sartans. J Hypertens 24: S23–S30.

Vauquelin G, Bostoen S, Vanderheyden P, Seeman P (2012). Clozapine, atypical antipsychotics and the benefits of fast-off D2 dopamine receptor antagonism. Naunyn Schmiedebergs Arch Pharmacol 385: 337–372.

Watson C, Jenkinson S, Kazmierski W, Kenakin T (2005). The CCR5 receptor-based mechanism of action of 873140, a potent allosteric noncompetitive HIV entry inhibitor. Mol Pharmacol 67: 1268–1282.

Wells JA (1990). Additivity of mutational effects in proteins. Biochemistry 29: 8509–8517.

Yao X, Parnot C, Deupi X, Ratnala VR, Swaminath G, Farrens D *et al*. (2006). Coupling ligand structure to specific conformational switches in the beta2-adrenoceptor. Nature Chem Biol 2: 417–422.

Supporting information

Additional Supporting Information may be found in the online version of this article at the publisher's web-site:

http://dx.doi.org/10.1111/bph.12683

Figure S1 Simulated association binding according to the one-step model; that is, the radioligand 'A'–receptor 'R' interaction is a simple, reversible bimolecular process obeying the law of mass action with $k_1 = 1 \times 10^7$ $M^{-1}{\cdot}min^{-1}$ for association and $k_{-1} = 5 \times 10^{-2}$ min^{-1} for dissociation. (A) Receptor occupancy at two concentrations of radioligand over a 60 min incubation period with data points (not shown) collected every 6 min. (B) k_{obs} values obtained by analysing curves such as in (A) according to monoexponential association binding model (GraphPad Prism 4.0; GraphPad Software Inc., San Diego, CA, USA) are plotted as a function of the free radioligand concentration (it is assumed that this concentration remains constant at all times).

Figure S2 Simulated association binding according to the two-step induced-fit model in where the initial RA complex slowly isomerizes into a tighter binding R'A complex with $k_2 = 2 \times 10^{-2}$ min^{-1} for isomerization and $k_{-2} = 2 \times 10^{-3}$ min^{-1} for reverse isomerization.

(A) Total and individual modes of receptor occupancy at [A] = 2 nM over a 60 min incubation period. (B) Total and individual modes of receptor occupancy at [A] = 8 nM. (C) k_{obs} values are obtained by analysing total occupancy [i.e. (RA) + (R'A)] curves such as in (A) and (B) for the indicated time lapses (10 equally spaced measurements each) according to monoexponential association binding model and plotted as a function of the free radioligand concentration. Inset: same plot but with k_{obs} values obtained by analysing [R'A] only.

Figure S3 Simulated dissociation according to (A) the one-step model and (B, C) the two-step induced-fit model with (B) for total binding and (C) for total binding as well as each individual mode of receptor occupancy. Receptors are pre-incubated with [A] = 8 nM for the indicated time periods and [A] is then set to 0 for the indicated time periods (abscissa) to simulate the washout. (A) Data are analysed according to a one-phase exponential decay model and (B) a two-phase exponential decay model to yield the respective $k_{off\text{-}fast}$ and $k_{off\text{-}slow}$ values as well as the amount of implicated receptors [in % of (R_{tot}) involved, listed in Supporting Information Table S1].

Figure S4 Simulated saturation binding according to (A) the one-step model and (B) the two-step induced-fit model. The incubation lasts for the indicated time periods and binding refers to total receptor occupancy [i.e. (RA) + (R'A)]. Curves

are analysed according to a variable slope sigmoidal dose–response model to yield the apparent pK_D values and Hill coefficients, n_H. Values are listed in Supporting Information Table S2.

Figure S5 Simulated competition binding according to (A, C) the one-step model and (B, D) the two-step induced-fit model. Radioligand: total binding (in % of control binding, i.e. binding in medium only) of the radioligand [(A) = 3 nM] is plotted as a function of the concentration of unlabelled competitive ligand, 'I'. This unlabelled ligand binds with the same rate constants as 'A' and can thus be considered to represent its unlabelled counterpart.

(A, B) Co-incubation experiments lasting for the indicated periods of time. (C, D) Receptors are first pre-incubated for 3 h with increasing [I] and then co-incubated with the same concentrations of 'I' and with [A] = 3 nM for the indicated periods of time.

Data are analysed according to a variable slope sigmoidal dose–response model to yield the apparent pIC_{50} values and Hill coefficients, n_H. Values are listed in Supporting Information Table S3.

Figure S6 Ratio between co-incubation and pre-incubation IC_{50} values of the competition binding curves shown in Supporting Information Fig. S5 (values are listed in Supporting Information Table S3) as a function of the (final) co-incubation time. The evolution of those ratios with time are compared for the one-step and two-step binding mechanisms. The ratios should be equal to 1 when equilibrium binding is attained.

Figure S7 Kinetic shifts (panel a) and pK_D values (panel b) of ligands what bind according to a two-step mechanism with the microkinetic rate constants for each step listed enumerated at the bottom.

Kinetic shift: the pre-incubation and incubation times were kept constant (i.e. 180 and 120 min, respectively) and the same ligand was used as radioligand and unlabelled competitor, and the concentration of the radioligand amounted three times its apparent K_D after 180 min incubation. Competition data are analysed according to a variable slope sigmoidal dose–response model to yield the apparent IC_{50} values.

pK_D values: $K_{D(2\text{-}step)}$ refers to the genuine 'macroscopic' K_D of the ligand defined as $K_D = k_{-1}{\cdot}k_{-2}/[k_1{\cdot}(k_2 + k_{-2})]$ (Tummino and Copeland, 2008). pK_D saturation refers to the apparent K_D of each ligand in question from the 180 min saturation binding experiments. Curves are analysed according to a variable slope sigmoidal dose–response model. pK_D association refers to the k_{off}/k_{on} values that can be obtained via the following equation ($k_{obs} = k_{off} + k_{on}{\cdot}[A]$). To calculate k_{obs}, from simulated association curves, receptors were incubated for 40 min with each ligand in question (with [A] = 3 × K_D saturation) and with receptor occupancy recorded every 4 min. Values for all ligands are listed in Supporting Information Table S4.

Figure S8 Representative dissociation curves. For the simulations, receptors were pre-incubated with each ligand for 30 min. The ensuing wash-out was then simulated by setting the free ligand concentration to zero and remaining receptor occupancy was recorded every 12 min for a total period of 120 min. Binding is presented as percent of binding at the onset of the washout. k_{off} values for all ligands (obtained by analysing the data of the data according to a biexponential decay model) are listed in Supporting Information Table S4.

Table S1 Binding parameters obtained by analysing the dissociation curves in Supporting Information Fig. S3. k_{-1} and k_{-2} values are the input dissociation and reverse isomerisation rate constants respectively. k_{off} values are obtained by analyzing the simulated dissociation data according to a one-phase exponential decay model (for one-step binding) and a two-phase exponential decay model (for two-step binding).

Table S2 Binding parameters obtained by analysing the saturation binding curves in Supporting Information Fig. S4a and b. n_H values are only given when (quasi) equilibrium binding is not yet reached (i.e. when $n_H \geq 1.05$).

Table S3 Binding parameters for the unlabelled ligand 'I' obtained by analysing the competition binding curves in Supporting Information Fig. S5. n_H values are only given when (quasi) equilibrium binding is not yet reached (i.e. when $n_H \geq 1.05$).

Table S4 See separate file. Input, microkinetic constants and calculated binding parameters for the control ligand and ligands 2–7. Dissociation kinetic data were obtained as outlined in the legend of Supporting Information Fig. S8. The 'Macroscopic' k_{off} was calculated by the equation $k_{off} = k_{-1}{\cdot}k_{-2}/(k_{-1} + k_2 + k_{-2})$ (Tummino and Copeland, 2008). The 'Macroscopic' K_D and Saturation K_D(app) values were obtained as outlined in the legend of Supporting Information Fig. S8.

Appendix S1 A study into the molecular mechanism of binding kinetics and long residence times of human CCR5 receptor antagonists.